

Alma Mater Studiorum Università di Bologna
Archivio istituzionale della ricerca

Shared micromobility-driven modal identification of urban bridges

This is the final peer-reviewed author's accepted manuscript (postprint) of the following publication:

Published Version:

Said Quqa, P.F.G. (2022). Shared micromobility-driven modal identification of urban bridges. AUTOMATION IN CONSTRUCTION, 134, 1-16 [10.1016/j.autcon.2021.104048].

Availability:

This version is available at: <https://hdl.handle.net/11585/839512> since: 2022-03-02

Published:

DOI: <http://doi.org/10.1016/j.autcon.2021.104048>

Terms of use:

Some rights reserved. The terms and conditions for the reuse of this version of the manuscript are specified in the publishing policy. For all terms of use and more information see the publisher's website.

This item was downloaded from IRIS Università di Bologna (<https://cris.unibo.it/>).
When citing, please refer to the published version.

(Article begins on next page)

Shared micromobility-driven modal identification of urban bridges

Said Quqa, corresponding author

Affiliation: Department of Civil, Chemical, Environmental, and Materials Engineering, University of Bologna, Viale del Risorgimento 2, 40136 Bologna, Italy

E-mail: said.quqa2@unibo.it

Pier Francesco Giordano

Affiliation: Department of Architecture, Built Environment and Construction Engineering, Politecnico di Milano, 20133 Piazza Leonardo da Vinci 32, Milan, Italy

E-mail: pierfrancesco.giordano@polimi.it

Maria Pina Limongelli

Affiliation: Department of Architecture, Built Environment and Construction Engineering, Politecnico di Milano, 20133 Piazza Leonardo da Vinci 32, Milan, Italy

E-mail: mariagiuseppina.limongelli@polimi.it

Abstract

Recent research in Indirect Structural Health Monitoring (ISHM) uses the dynamic response of instrumented vehicles to carry out “drive-by” monitoring of bridges. These vehicles are generally cars or trucks instrumented with different types of sensors. However, some urban bridges are inaccessible to regular vehicles. Also, cars and trucks have non-negligible weight and suspension systems that may affect the collected vibration data. Stiff, light, and standardized shared micromobility vehicles, such as bicycles and electric kick scooters, have never been explored for ISHM purposes. This paper proposes an innovative and automatic ISHM strategy based on the data collected by smartphones temporarily installed on shared micromobility vehicles. An identification procedure suitable for cloud computing is proposed to extract the dynamic parameters of bridges without needing any sensor deployment, becoming particularly appealing for monitoring a densely built environment at a territorial scale. The methodology is applied to a real footbridge in Bologna (Italy).

Keywords: smart city, indirect structural health monitoring, modal identification, crowdsensing, data fusion, footbridge.

1. Introduction

Infrastructure maintenance is a concern for transport authorities due to the increasing number of structures reaching the end of their design lifespan, the need to optimize the allocation of economic resources during structural maintenance activities, and the growing intensity of natural calamities related to climate change, which accelerate degradation phenomena.

Nowadays, the state of health of civil infrastructures is assessed by specialized technicians through visual inspections and testing campaigns. As an alternative, Structural Health Monitoring (SHM) methods have been developed in the last decades [1]. Existing SHM techniques usually employ sensing devices (consisting of sensors, cables, and acquisition systems) directly installed on structures. Damage-sensitive features are extracted by analyzing physical measurements, which allow tracking the health conditions of the analyzed structure in time. Among SHM techniques, vibration-based SHM employs the dynamic response of structures (e.g., acceleration or velocity measurements collected at instrumented points) to retrieve information about their performance over time [2]. The main advantage of vibration-based SHM methods is that they provide information about the structural conditions even if the sensors are not close to the damage location [3–6]. Moreover, the structural integrity can be assessed remotely, without the physical presence of operators. The drawbacks of traditional SHM systems generally relate to their installation cost, which is strongly influenced by the typology and number of the sensors employed. Moreover, an accessible power source must be available in the proximity of the monitored structure, and the different components require continuous maintenance, involving additional costs during the lifecycle of the SHM system. Besides, SHM systems are not widespread due to the difficulty of estimating their economic benefit over the initial investment [7,8].

Recent studies conducted on Indirect vibration-based Structural Health Monitoring (ISHM) exploit the dynamic response of instrumented vehicles to identify structural parameters. In principle, the use of passing vehicles simplifies the monitoring process and cuts the cost associated with the installation of SHM systems. The idea of using sensors installed on moving vehicles was initially explored theoretically by Yang et al. [9] in 2004. Specifically, the authors proposed using an instrumented vehicle both as an exciter and a receiver of the structural response. Lin and Yang [10] subsequently demonstrated the possibility of applying this approach in practice. The authors used a tractor-trailer system to identify the first natural frequency of the Da-Wu-Lun Bridge, a prestressed concrete girder bridge in Taiwan. The tractor consisted of a four-wheel commercial light truck, and the trailer was a two-wheel cart. The tractor acted as an exciter while the accelerometers applied to the cart served as receivers. Kim and Kawatani [11] extended this concept to identify structural damage in bridges, introducing the “drive-by bridge inspection”. In their work, the authors identified the change in fundamental frequencies due to structural damage in a scaled laboratory model. A few years later, Cerda et al. [12] called this concept “indirect SHM”, in contrast to the “direct SHM”, where measurements are collected directly on the structure.

After that, a growing number of scientific papers have proposed several ISHM approaches in terms of different exciter-receiver configurations. Kim et al. [13] suggested using a tractor and two identical instrumented trailers to improve the estimation of the dynamic properties of the bridge. Li et al. [14] developed an ISHM strategy based on two instrumented vehicles in which the first is used as a fixed reference sensor while the other is a moving sensor. Kim et al. [15] proposed a two-stage wireless monitoring strategy relying on vibrational data provided by sensors installed both on a passing vehicle and on the bridge. Matarazzo et al. [16] suggested using crowdsourced data collected by automobiles used as the nodes of large-scale sensor networks for bridge monitoring.

In the last fifteen years, several ISHM methods for bridges based on vibration signals have been formulated theoretically and tested on numerical models [17–19] and laboratory-scale experiments [20–22]. Several studies validated ISHM techniques on real structures, such as cable-stayed [23], continuous steel box girder [15], simply-supported box girder [24], simply-supported steel truss [25], and prestressed concrete girder [10,26] bridges. These studies employed a variety of vehicles for in-situ SHMI applications, such as cars [27], vans [24], trucks [15], tractor-trailer systems [10], busses [28], and even hand-drawn carts [23]. References [29–31] provide comprehensive reviews on ISHM methods for bridges. Specifically, Zhu and Law [29] reviewed SHM methods based on vehicle-bridge interaction. Malekjafarian et al. [30] focused on modal identification, observing that mode shapes are the most complex features to identify. Also, they concluded that the main challenges for indirect bridge monitoring are related to the road profile, the limited recording time, and the presence of environmental effects. Shokravi et al. [31] presented a review that includes vision-based, weigh-in-motion, bridge weigh-in-motion, drive-by, and vehicle bridge interaction-based methods.

Very recently, low-cost ISHM strategies based on the use of data collected by smartphones have been proposed. Feng et al. [32] investigated the reliability of smartphone accelerometers for vibration-based direct SHM, while, a few years later, McGetrick et al. [33] explored drive-by monitoring systems incorporating smartphones. Both the studies have shown promising results for drive-by and, generally, SHM applications. To address the issue of the low sensitivity and high noise floor of smartphone sensors, Elhatab et al. [34] proposed a stochastic resonance filter that enables identifying the resonant frequencies of weak signals. In their study, the first four natural frequencies of a bridge are successfully identified using a smartphone. Ozer et al. [35] proposed an approach to extract modal parameters in a similar noisy environment, also dealing with synchronous and sampling-deficient measurements.

Recent smartphones include high-performance batteries and have advanced cellular transmission modules that keep them constantly connected to the Internet, generating continuous transmission traffic. The ubiquity of these devices has provided an opportunity to implement crowdsensing strategies [36,37]. Ozer et al. [38] have shown the possibility of identifying structural modal properties with high accuracy using measurements collected by citizens without expertise. Ozer and Feng [39] explored the potential of using vibration data measured by pedestrians to identify modal parameters of bridges. A few years later, the same authors [40] experimented with a finite element model updating strategy using

vibration data obtained from smartphones. Matarazzo et al. [41] gathered data from UBER riders crossing the Golden Gate Bridge in San Francisco, California, to retrieve the main modal parameters of the structure, which in turn can provide valuable information concerning the health state of the structure. Due to the short duration of typical tests conducted in most of the mentioned studies, accurate vehicle-bridge interaction with road roughness modeling is generally necessary to obtain significant results from the collected measurements. This is one of the most critical limitations of heavy vehicles that also affect the structural dynamics and generate nonstationary excitation, which is typically incompliant with the underlying assumptions of traditional SHM algorithms.

Smartphones have several built-in sensors, generally including an Inertial Measurement Unit (IMU) and a Global Positioning System (GPS) module. Some authors proposed approaches for the identification of bridges through heterogeneous data fusion [42,43]. Ozer et al. [44] presented a method to keep track of the orientation changes of the sensor by integrating different measurements collected through gyroscope, accelerometer, and magnetometer.

Applications using data collected by smartphones are not limited to drive-by monitoring of road bridges. For instance, Feng et al. [32] proposed a smartphone-based crowdsensing network for rapid and low-cost post-earthquake damage assessment of structures and infrastructure at a city-scale, while Seraj et al. [45] and Chuang et al. [46] developed methodologies to evaluate the state of road pavements. In different recent applications, the data collected by other smart wearable devices was fused to estimate crowd flow and load on pedestrian bridges [47].

To the authors' knowledge, the widespread Human-Powered Vehicles (HPVs), such as bicycles and kick scooters, have never been considered in the relevant literature for ISHM. The main advantages of these types of vehicles are their low cost, high sustainability [48], and the environmental benefits they provide in urban areas reducing traffic congestion [49]. Also, light vehicles generally have low speed and negligible mass with respect to the monitored structures and do not affect their dynamic behavior. Moreover, HPVs allow monitoring structures that are not accessible by cars and trucks, such as footbridges. Nevertheless, noise effects introduced by the driver, as well as the vehicle dynamics and the uncertainty of the data recorded by smartphones (that are generally equipped with low-cost sensors), may affect the data recorded on HPVs. However, the availability of crowdsourcing data could considerably improve the overall quality of the obtained ISHM results, especially if all the users employ standard vehicle types, i.e., if the vehicle properties are known. Shared micromobility vehicles, such as bike and scooter sharing services, could be particularly useful to this purpose since sharing companies generally provide very few vehicle types in a certain urban area.

This paper extends the available knowledge on ISHM techniques, exploring the possibility of using unconventional vehicles, i.e., HPVs, for infrastructure monitoring purposes. Specifically, the feasibility of using bicycles to extract modal or operational parameters commonly employed by vibration-based SHM methods, i.e., natural frequencies mode shapes or operating deflection shapes (ODSs), is demonstrated on a footbridge located in Bologna, Italy. This research lays the foundations for a human-

centered monitoring approach of urban bridges based on shared micromobility vehicles and smartphones.

The paper is organized as follows. In Section 2, the proposed monitoring strategy is described in the context of a widespread micromobility-based application, highlighting the positive aspects that the urban environment and society could gain. Section 3 technically details the methodology proposed to fuse data acquired by the several smartphone built-in sensors into dynamic damage-sensitive features, usable for SHM of urban infrastructures. Section 4 presents the case study investigated in this paper, namely a footbridge for pedestrians and bicycles. The experimental setup, entailing several data acquisition scenarios related to different user activities, is described. This section reports the identified dynamic parameters that could be further employed for the identification of structural anomalies. The paper concludes with the final remarks.

2. Shared micromobility-oriented monitoring strategy

In general, using a smart monitoring system involves a migration from the traditional planned maintenance, which may involve unnecessary expenses, to condition-based maintenance, performed when certain indicators show signs of decreasing performance or impending failure. While the common practice in SHM is to periodically measure the structural response (e.g., displacements or accelerations) using dedicated sensors, new crowdsourcing strategies based on smartphone data can be highly convenient, especially for applications at a territorial scale. Smartphones are now essential elements even while driving or walking around cities, as they offer turn-by-turn navigation information, travel times, and route details. Besides, in the context of an SHM strategy, built-in GPS and IMU sensors can provide helpful information on the precise position of the vehicle, its velocity, and vibration data.

An ever-increasing number of social networks and “community-driven” GPS navigation services have shown that a human-centered system can actively contribute to the crowdsourcing of valuable data to improve or provide accurate information on the environment around us [50]. The significant diffusion of smartphones enabled citizens to become the carriers of distributed sensing devices, being themselves the smart sensors of cities and transportation infrastructure.

The sector of shared micromobility (i.e., bike sharing and scooter sharing services) is incredibly expanding in several areas of the world [51]. Combined with the enormous potentialities of smartphones as sensing devices, this phenomenon opens up new avenues for ISHM, especially considering that, in this case, sensing devices are free for the infrastructure owner. This economic saving can be devolved to motivate the users to use shared vehicles and thus provide monitoring data through rewards and discounts. A “gamification” of the monitoring process has already shown particularly effective in this context [52]. Moreover, from a social viewpoint, this strategy would create a human-centered monitoring paradigm to promote the civil sense and raise the awareness and protection of the built

inheritance, fostering a sustainable approach for managing the urban environment based on maintenance.

Regarding the technical aspect, smartphones already have dedicated applications that enable users to unlock and use shared vehicles. Integrating these applications with recording, processing, and transmission tools is straightforward since most health and navigation apps already collect data in full respect of privacy. In the framework of the envisioned application, the mobile app should autonomously interact with a cloud-based backend solution in charge of carrying out the analyses required and provide feedback to involved stakeholders.

The monitoring strategy proposed in this paper aims at achieving both the optimization of maintenance operations, resulting in minor management costs and safer roads and infrastructures: The installation of sensors on civil infrastructures that becomes particularly expensive when their number is large in a densely built area, is avoided, also cutting the costs related to their maintenance and management. Moreover, information on the state of health of urban bridges can help to identify anomalies and adopt an “on-demand” maintenance policy, thus resulting in generally safer infrastructures and more effective maintenance procedures. This strategy also promotes the shared micromobility as an alternative and sustainable transport system within cities. In principle, smartphones installed on shared vehicles could be used for various monitoring applications in the built environment, including assessing the health of road bridges, footbridges, and the state of road pavements [46]. This paper focuses on identifying dynamic parameters of urban infrastructures (bridges and footbridges) that can be employed to automatically detect structural anomalies that may undermine the functionality of these key elements of the city traffic network. Although the practical development of a mobile application with a cloud-based backend solution is beyond the scope of this work, this paper shows the theoretical framework and the experimental results that demonstrate the applicability of the proposed monitoring strategy.

3. Dynamic identification procedure

In this section, a procedure to estimate dense (i.e., with high spatial resolution) dynamic structural features from the set of data collected using smartphones is proposed. The procedure processes the data collected by several smartphones, each fixed on a vehicle moving on the bridge, continuously acquiring data during the passage on the bridge.

Most smartphones in commerce have built-in GPS and IMU sensors, such as MEMS accelerometers, gyroscopes, and magnetometers. Several mobile applications use the data measured by such sensors to provide the users with route indications and other interactive functions. Since strict synchronization of different data types is unnecessary for most traditional applications, the data is typically collected asynchronously. Moreover, GPS measurements are generally less frequent than IMU recordings to optimize the power management of mobile devices.

Considering the time interval delimited by the instants t_0 and t_T when the vehicle enters and leaves the bridge, respectively, assume that a mobile application installed on a smartphone generates a vector \mathbf{z}_k as soon as a measurement is collected (say, at the k -th instant). The vector \mathbf{z}_k can contain information about the acceleration and the angular velocity collected along three orthogonal axes, three magnetic field measurements, and three position logs, including latitude, longitude, and altitude. Since data is generally measured asynchronously, the vector \mathbf{z}_k has a varying size in time. Specifically, $\mathbf{z}_k \in \mathbb{R}^M$, where M is the variable number of measurements.

To analyze smartphone measurements collected on the bridge, the time interval $[t_0, t_T]$, during which the vehicle is physically on the bridge, should be first identified. Most civil infrastructures have statically determined schemes guaranteed by expansion joints that accommodate sliding movements of the restraints. A smartphone deployed on a moving vehicle that crosses a bridge will likely experience vertical acceleration peaks at the vehicle passage through expansion joints. These peak accelerations in the neighborhood of the ends of the bridge (which are easily accessible through built-in GPS sensors) make it possible to identify time instants t_0 and t_T accurately. This procedure exploits a simple yet effective approach to extract precisely the time histories of GPS and IMU recordings corresponding to the bridge crossing. However, if the bridge has no expansion joints, the GPS data can be used to select an approximate interval of the measurement time histories included between two geographical points identified as the bridge ends.

The data measured by each smartphone during its travel on the bridge in the interval $[t_0, t_T]$ (that vary for each vehicle), is stored in a cloud database and processed according to the procedure illustrated on the right-hand side of Figure 1. Since smartphones are generally connected to the Internet, this procedure is particularly suitable for crowdsourced cloud computing applications. Specifically, it includes the following operations:

- 1) Identification of the sensor location: The GPS and all the IMU measurements, except the vertical accelerations, are used to estimate the vehicle (and sensor) location with a high spatial resolution;
- 2) Identification of the bridge dynamic features: The vertical accelerations are used to retrieve the features (in terms of resonant frequencies and modal amplitudes) of the dynamic response of the bridge;
- 3) Estimation of the average modal amplitude components: The dynamic features, identified at positions that depend on the specific path of the vehicle, are realigned at the locations identified at point (1); this way, the modal amplitudes identified by different vehicles can be averaged.

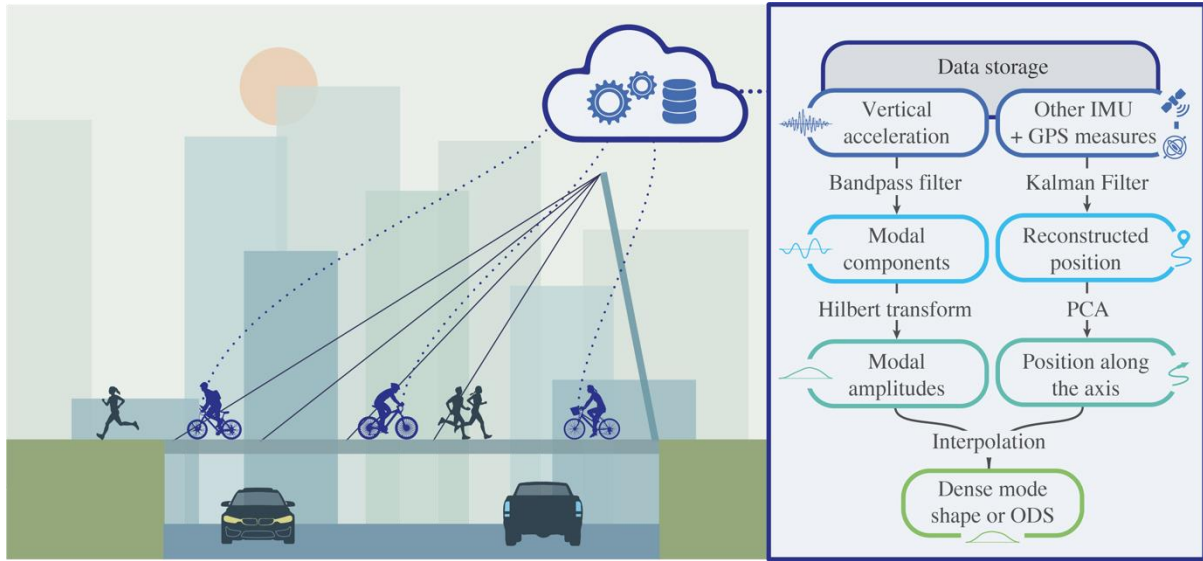


Figure 1 Scheme of the proposed procedure

Specifically, IMU and GPS data are fused through an extended Kalman filter to obtain the vehicle position along the axis of the bridge. Simultaneously, a band-pass filter is used on the vertical acceleration data to obtain the instantaneous dominant frequency and the amplitude (here addressed to as “modal amplitude”) of the structural response in a user-determined frequency Range of Interest (RoI). The RoI is determined before the crowdsourcing application commences, based, e.g., on previous monitoring data or an available finite element model of the monitored structure, and its boundaries are selected to include the resonant frequency of a vibration mode of interest. The proposed procedure calculates the amplitudes of the modal or Operational Deflection Shapes (ODSs) with high spatial resolution and can provide a more accurate estimate of the dominant resonant frequency within the RoI.

It should be noted that, since the measured datasets (here called “samples”) are relevant to different vehicles, both the length of the time histories and the positions where the data are measured change with the speed of the vehicle and its specific path. A realignment procedure of dynamic features is proposed herein to interpolate this data to a user-defined spatial grid along the bridge axis. Thanks to the distributed data collection through crowdsensing, several data samples are available and provide a large set of identified modal amplitudes. The averaging of these estimates can improve their robustness by mitigating the unavoidable noise component contained in each of them. The steps of the proposed method are described in detail in the following subsections.

3.1 Identification of the sensor location

The Extended Kalman Filter (EKF) is a widely used iterative tool for combining uncertain measurements to obtain accurate information about nonlinear dynamic systems [53]. In particular, the nonlinear equations that describe the evolution of the state of the system (state transition model) and its relationship with the measurements (observation or measurement model) are linearized locally by

computing their Jacobians. If the measurements collected to update the state of the EKF are acquired asynchronously and with a varying sampling frequency, as it usually happens in smartphones, a Continuous-Discrete version of the EKF (CD-EKF) can be employed. In this case, the evolution of the state is described as a continuous function (in particular, a stochastic differential equation) and is updated as soon as a new measurement is collected [54]. In this paper, the symbol $\mathbf{x}(t)$ denotes a vector dependent on continuous time, while \mathbf{x}_k is the discrete value of \mathbf{x} at time t_k , i.e., the instant when measurements are taken.

The system and measurement models of the CD-EKF assumed in this study are described, respectively, by the following equations:

$$\dot{\mathbf{x}}(t) = g(\mathbf{x}(t)) + \mathbf{w}(t) \quad (1)$$

$$\mathbf{z}_k = h(\mathbf{x}_k) + \mathbf{v}_k \quad (2)$$

where \mathbf{z}_k is the vector containing the discrete measurements; $\mathbf{x}(t)$ and its discrete version $\mathbf{x}_k = \mathbf{x}(t_k)$ are vectors containing the state variables; $\mathbf{w}(t) \sim \mathcal{N}(\mathbf{0}, \mathbf{Q}(t))$ and $\mathbf{v}_k \sim \mathcal{N}(\mathbf{0}, \mathbf{R}_k)$ are the process and observation noise, respectively, both assumed as zero-mean multivariate Gaussian noise processes with covariance matrices $\mathbf{Q}(t)$ and \mathbf{R}_k . The differentiable nonlinear functions $g(\mathbf{x})$ and $h(\mathbf{x})$ are the state transition and the observation function, respectively.

In this study, a 28-element state vector is employed to track the orientation (expressed as the four elements of an orientation quaternion), the velocity, the position, the Magnetic, Angular Rate, Gravity (MARG) sensor biases, and the geomagnetic vector. Moreover, the initial state $\mathbf{x}(t_0)$ and the noise vectors $\mathbf{w}(t)$ and \mathbf{v}_k at each time t are assumed as mutually independent. Appendix A of this paper shows the structure of the state vector, the state transition function, and the observation functions.

In the EKF procedure, two steps, namely the prediction and update steps, alternate, with the prediction continuously advancing the state until the next measurement becomes available. From a practical point of view, although the state transition model assumed in the CD-EKF is continuous, prediction steps are carried out at discrete (yet arbitrary distanced) time instants. In this study, a constant frequency f_s equal to the sampling frequency of the vertical acceleration is selected for this purpose. This is meant to estimate the state parameters at the time instants when the vertical acceleration is measured. More numerical details on this aspect are given in Section 4 and Appendix B.

In the update step, the a priori prediction of the current state is combined with the measurement collected at time t_k to refine its estimate. It should be noted that, while $g(\mathbf{x})$ has a fixed size, depending on the structure of \mathbf{x} , the observation function $h(\mathbf{x})$ has a size that depends on the variable structure of \mathbf{z}_k . In Appendix A, the different structures for the function $h(\mathbf{x})$ are reported for each possible measurement. Also, more details on the EKF implementation for the application described in this paper are provided in Appendix B.

Upon calculating the estimated state vector in the interval $[t_0, t_T]$ with a sampling frequency f_s , here indicated as $\hat{\mathbf{x}}$, the estimated position information $\hat{\mathbf{y}}$ contained in $\hat{\mathbf{x}}$ is organized in a reconstructed

position matrix $\mathbf{Y} = [\hat{\mathbf{y}}_0, \dots, \hat{\mathbf{y}}_T]^T \in \mathbb{R}^{N \times 3}$ where N indicates the number of instants in the interval between t_0 and t_T . In particular, the vector $\hat{\mathbf{y}}$ consists of the position of the smartphone obtained by converting into local coordinates the position in geodetic coordinates (i.e., latitude, longitude, and altitude) contained in the state vector. Specifically, the geodetic coordinates are the elements from 14-th to 16-th of the state vector reported in Appendix A. The origin of the local coordinates system (defined in north-east-down format) is assumed at the midspan of the bridge.

For the purposes of the presented algorithm, it is convenient to express the location information along the bridge axis. If the structure analyzed has a straight axis, the position data can be efficiently projected onto it by extracting the first principal component from the dataset \mathbf{Y} . Specifically, let the singular value decomposition (SVD) of \mathbf{Y} be

$$\mathbf{U}\mathbf{\Sigma}\mathbf{V}^T = \mathbf{Y} \quad (3)$$

where $\mathbf{U} \in \mathbb{R}^{N \times N}$ and $\mathbf{V} \in \mathbb{R}^{3 \times 3}$ are the matrices containing the left singular vectors and right singular vectors of \mathbf{Y} , while $\mathbf{\Sigma} \in \mathbb{R}^{N \times 3}$ is the diagonal matrix of singular values. It should be noted that, since \mathbf{Y} is formed of three column vectors representing the position in the local coordinate system, the projection of the three-dimensional position data onto the principal direction, that is, the direction in which the position data explains the higher variance (i.e., the axis of the bridge), can be calculated as

$$\mathbf{y} = \mathbf{U}\mathbf{\Sigma}\mathbf{s} \quad (4)$$

where the vector $\mathbf{s} = [1, 0, 0]^T$ simply extracts the first principal component (i.e., the first column vector) from the matrix $\mathbf{U}\mathbf{\Sigma}$. This way, the vector $\mathbf{y} = [y_0, \dots, y_T]^T$ contains the dense estimates of the position of the sensor for the entire time interval when the vehicle crosses the bridge.

3.2 Identification of the bridge dynamic features

This section describes the identification of the dynamic structural parameters (i.e., natural frequencies and modal amplitudes) from the vertical acceleration recorded by a single smartphone.

Let the structural response collected on the moving vehicle in terms of vertical acceleration \ddot{u} be:

$$\ddot{u}(y, t) = \sum_{i=1}^{\infty} \phi_i(y) \ddot{q}_i(t) \quad (5)$$

where $\phi_i(y)$ is a component of the i -th mode shape function at location y and $\ddot{q}_i(t)$ is the double derivative of the i -th modal contribution to the structural displacement.

Let $b_p(\tau)$ be the impulse response of a band-pass filter $b_p(\tau)$ having low and high cutoff frequencies equal to $f_l = f_p - \varepsilon$ and $f_h = f_p + \varepsilon$, respectively, where f_p is the central frequency of the selected interval (i.e., the frequency RoI) and ε is a small number. Consider a slow vehicle (compared to the oscillating velocity of the structure) and well-distanced vibration modes. If f_p coincides with the p -th resonant frequency of the structure, applying the filter $b_p(\tau)$ to the acceleration response, the modal

contributions with $i \neq p$ are canceled [55,56] and a narrow-band signal, with frequency content close to the p -th mode is obtained:

$$(\ddot{u} * b_p)(y, t) = \sum_{i=1}^{\infty} \phi_i(y) (\ddot{q}_i * b_p)(t) \cong \phi_p(y) \ddot{q}_p(t) \quad (6)$$

The amplitude $a_p(y, t)$ of the structural response can be calculated as the absolute value of the analytic signal obtained from Eq. (6) using the Hilbert transform [57]. Assuming the excitation of the bridge as a stationary and uncorrelated white noise process, different vehicles crossing the bridge at different times are all subject to different vibration amplitudes at a given location y_k (and corresponding time t_k). While the term $\phi_p(y_k)$ is the same in all the cases, the input excitation and, consequently, $\ddot{q}_p(t_k)$ varies randomly. Therefore, averaging the amplitude of the filtered signals extracted from different samples (measured by different vehicles passing on the bridge), it is possible to obtain the p -th mode shape $\phi_p(y)$, except for a normalization factor. It is observed that the location of the vehicle is a function of its velocity and time. Then, to correctly average the modal amplitudes, the measurements of different vehicles must be defined at the points of a unique spatial grid. This aspect is detailed in Section 3.3. It is also noted that the Hilbert transform provides the absolute value of the instantaneous amplitude. Thereby, the absolute values of the mode shapes are identified in this procedure.

If the central frequency f_p of the filter is not coincident with a resonant frequency of the structure or closely spaced modal contributions are included in the RoI $[f_l, f_h]$, $\phi_p(y)$ represents the average of the ODSs included in $[f_l, f_h]$. Nevertheless, in the proximity of one or more resonant frequency peaks, the ODS can also be used as a damage-sensitive feature for SHM purposes [58,59].

The proposed method provides a more accurate estimate of the dominant frequency within the RoI through a simple peak-picking procedure on the frequency spectrum of the vertical acceleration data, carried out, e.g., considering the maximum spectral amplitude within the RoI. An instantaneous estimate of the resonant frequency within the RoI can also be identified from the filtered acceleration data using the Hilbert transform [57,60]. The time-dependent frequency obtained in this way can be averaged over time to obtain a single value of the dominant resonant frequency. If the structure is formed by independent spans, this procedure can be applied separately to each of them, extracting the frequency values from signals recorded on spatial subdomains corresponding to the different structural elements. The cutoff frequencies of the band-pass filter $b_p(\tau)$ – i.e., the boundaries of the RoI – should enclose a range of frequencies large enough to accommodate the variation of the resonant frequency due, for example, to varying environmental conditions. Indeed, the proposed method is able to operate with frequency shift within the frequency RoI. Nevertheless, higher frequency variations would be identified by the disappearance of the peak.

Multiple RoIs can be employed to identify different modes. However, the structure should be sufficiently excited in all the frequency RoIs to allow a reliable identification using the relatively low-performance sensors embedded into smartphones.

3.3 Estimation of the average modal amplitude components

In general, different vehicle speeds and changes of speed of a given vehicle lead to a variable spatial resolution of the modal amplitudes identified in Section 3.2 between samples and to a non-uniform spatial resolution for the same sample. This hampers their direct averaging. In order to compute the amplitudes $a_p(y, t)$ at the same points of a fixed spatial grid that is unique for all the vehicles, a linear interpolation of the shapes computed according to the procedure shown in Section 3.2 is carried out at equally spaced locations along the longitudinal axis of the bridge.

Let $\mathbf{a}_p = [a_p(y_0, t_0), \dots, a_p(y_T, t_T)]$ be a set of acceleration amplitudes measured by a moving vehicle at the instants t_k in the interval $[t_0, t_T]$ with a constant sampling frequency f_s , where y_0 and y_T are the start and end locations of the measurement. Moreover, consider the vector $\mathbf{y} = [y_0, \dots, y_T]^T$ of sensor location identified in the same interval according to the procedure presented in Section 3.1. Each couple of elements $(y_k, a_p(y_k, t_k))$ relates a physical location on the bridge y_k with the amplitude value a_p measured at that location at a time t_k . These couples are used to interpolate the data collected during the recording interval $[t_0, t_T]$, at equally spaced physical locations \bar{y}_k chosen within the spatial interval $[y_0, y_T]$.

This procedure allows estimating the amplitudes $a_p^s(\bar{y}_k)$ for each sample $s = 1, \dots, S$, that is for each measurement collected by a smartphone, at the same points \bar{y}_k and to obtain the average values of the shapes at locations \bar{y}_k :

$$|\phi_p(\bar{y}_k)|C \cong \frac{1}{S} \sum_{s=1}^S a_p^s(\bar{y}_k) \quad (7)$$

where C is a scale factor constant over y . It should be noted that the accuracy of the estimate increases with S ; thereby, the crowdsourcing nature of the proposed approach acquires fundamental importance. Local variations of such average amplitudes can be used to identify anomalies in the modal profile (e.g., damage due to local stiffness reduction) through one of the several methods proposed in the literature based on mode shapes or ODSs [2,59,61].

4. A case study

The methodology presented in Section 3 to obtain the main dynamic features of a bridge is applied in this section to a real case study to demonstrate its feasibility. Specifically, a smartphone fixed on a common city bicycle crossing a lively footbridge is used to collect multiple data types in different data

acquisition scenarios that can occur in practice. A single bicycle model was employed during the tests to simulate the use of a standard shared vehicle, which is the same for all the users. The dynamic response of this type of structure under operational loads is generally high enough to overcome the high noise floor of standard smartphone sensors. Crowdsourcing data is obtained by repeating the analysis several times. The results of the analysis (modal amplitudes and the first natural frequency) are compared to those obtained by other researchers during a vibration test using a traditional technique.

4.1 Description of the footbridge

The investigated case study is a footbridge for both pedestrians and cyclists, which crosses the A13 motorway between Bologna-Padova (Italy) in the proximity of the entrance to the Bologna ring road (see Figure 2). Detailed information on this structure can be found in Reference [62].

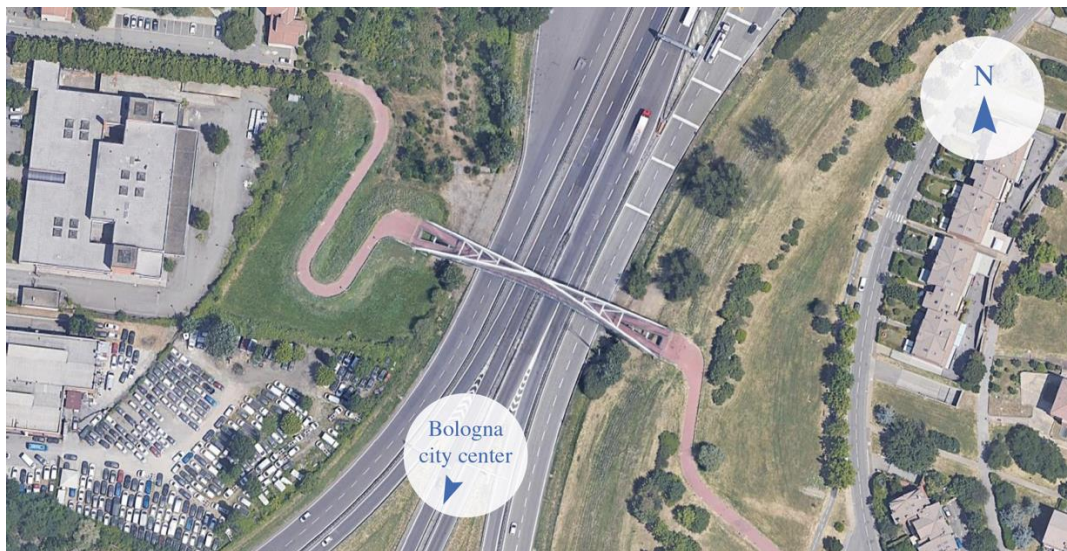


Figure 2 Aerial view of the case study

The overall free span of the footbridge is about 90 m (Figure 3a). The primary structural system is a three-hinged tied arch formed by two A-shaped steel frames contrasting at the center of the footbridge (Figure 3b). The arch rise is 20 m at midspan, and the minimum distance between the deck and the motorway level is 6 m. The width of the deck varies between 10 m at the two ends and 2.5 m at the midspan. The A-shaped frames present a tubular cross-section with variable dimensions obtained by welding different S355 steel plate elements. The bridge deck balances the horizontal thrust generated by the arch. A fan-shaped cable-stayed system converging to the center of the arch supports the deck (Figure 3c). A system of stabilizing ropes contributes to enhancing the structural behavior for gravitational loads and wind-related effects along the deck. The deck is supported at its ends by two reinforced concrete abutments. As for the external anchoring system, the four supports of the A-shaped steel frames prevent vertical displacements and rotations along the longitudinal axis of the deck. Moreover, two transversal restrains located on the abutments along the longitudinal axis of the

footbridge prevent the transversal displacements. Four visco-elastic damper actuators (Domain-Jarret type), which only allow slow displacements, control the structural displacements in the longitudinal direction due to thermal action, and prevent large displacements due, for instance, to earthquakes or wind. Drilled piles make the foundation system. The road surface of the footbridge is made of a plastic material (Figure 3b) and therefore is relatively smooth.

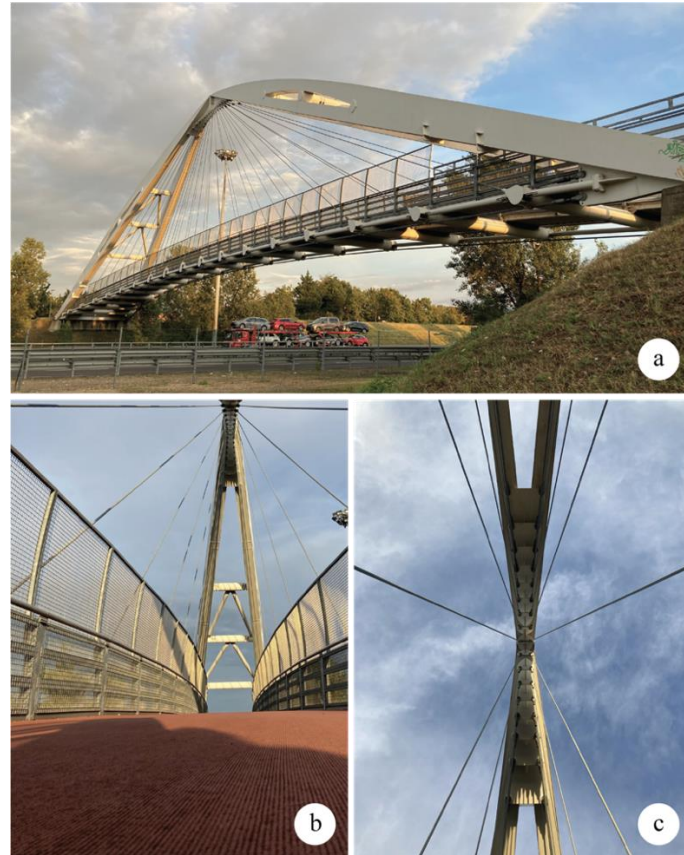


Figure 3 Case study: (a) Lateral view (Northside), (b) A-shaped frame and detail of the deck pavement, (c) Cable-stayed system

In the past, vibration tests have been carried out on the footbridge to estimate the main mode shapes and frequencies. The results are presented in Reference [63] and reported in Figure 4. Two closely spaced bending modes have been identified: The first presents a symmetrical mode shape, whereas the second shows an anti-symmetric mode shape.

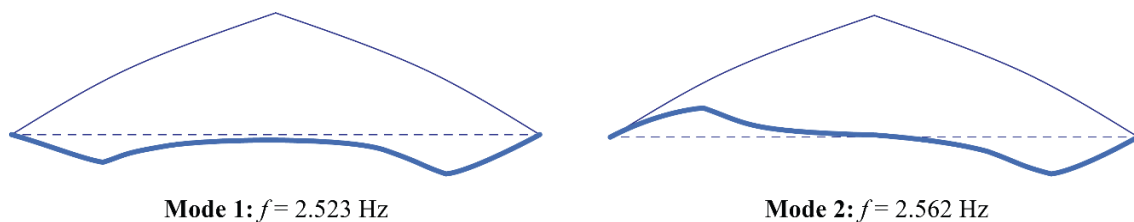


Figure 4 Results of the dynamic tests (adapted from [63])

4.2 Experimental setup

Experimental tests have been performed using a common city bicycle (Figure 5a), a smartphone, and support (Figure 5b) to fix the device to the vehicle (Figure 5c). During the tests, the pressure in the inner tube of the bicycle wheels was about 203 kPa (2 atm). The temperature measured at the test location was between 15°C and 21°C. However, further tests conducted with -2°C have shown that the environmental effects did not perceptibly affect resonant frequencies of the bridge. The following measurements have been acquired and used in this study: Triaxial acceleration, triaxial angular velocity, triaxial magnetic field, position in terms of latitude, longitude, altitude, together with the horizontal GPS accuracy, employed to determine the variance of the GPS measurements. A time stamp in the reference time of the mobile device is collected along with each measured quantity and employed in the KF to perform data fusion. A “calibration” sample, measured by the smartphone mounted on the bicycle standing, not in movement, was used to compute the error variances of the other measurement. The relevant values are reported in Table 1. The sampling frequency is 100 Hz for IMU data and 1 Hz for GPS data. The smartphone used during the tests is an iPhone SE (second generation, 2020) connected to the Internet. It includes a 16-bit 6-axis Bosch Sensortec IMU module with a typical accelerometer sensitivity of 16384 LSB/g at a recording range of $\pm 2g$ [64,65]. The results reported in the paper have been obtained using measurements recorded by a single phone. In a preliminary phase of the investigation test, different smartphones were used to assess the correct functioning of the GPS and IMU modules.



Figure 5 Instrumented bicycle: (a) Side view, (b) Smartphone support, (c) Detail of the smartphone position

Table 1 Reading error variance

Measurement	Variance
Acceleration	$0.01 \text{ m}^2/\text{s}^4$
Angular velocity	$0.001 \text{ rad}^2/\text{s}^2$
Magnetic field	$50 \text{ } \mu\text{T}^2$
Position (average)	25 m^2

The measurements have been acquired using the MATLAB Mobile app [66], which allows recording data from the different sensors of the smartphone and transmitting them directly to the MathWorks Cloud. This way, the data is directly transmitted to a Personal Computer (PC), where the algorithm operates.

Four types of tests have been carried out. Each test aims at simulating a distinct cyclist's behavior and, in turn, a data acquisition scenario that could occur in practical applications. The tests differ in terms of smartphone location, bicycle use, and recording length. Precisely:

- Test type 1: 36 data samples (18 in each direction) were collected riding back and forth the bicycle across the footbridge with the smartphone fixed to the top tube, as shown in Figure 5c. The duration of each sample ranges between 45 and 70 s (depending on the user's velocity). This test type simulates the typical situation in which a cyclist crosses the footbridge.
- Test type 2: 4 data samples (2 in each direction) were collected walking the bicycle back and forth across the footbridge with the smartphone fixed to the top tube, as shown in Figure 5c. The approximate duration of each sample is 100 s. This test type simulates the behavior of a cyclist who crosses the bridge walking instead of riding (for instance, due to the difficulty of overcoming the deck slope by riding the bicycle).
- Test type 3: 1 data sample collected while the bicycle was standing on the footbridge with the smartphone fixed to the top tube, as shown in Figure 5c. The recording time is 5 minutes. This test type simulates the behavior of a cyclist who stops on the footbridge (for instance, to start a conversation with somebody) while recording data.
- Test type 4: 1 reference data sample with the smartphone placed directly on the bridge (at 1/4 of the bridge span from the eastern support). The recording time is 5 minutes.

The main characteristics of the different tests are reported in Table 2. During all the tests, the bridge was quite lively: All tests have been carried out in operational conditions, with at least one pedestrian or a runner crossing the bridge. Vibration generated by moving people and vehicular traffic in the motorway underneath the footbridge contributed to exciting the structure during the tests.

Table 2 Test types

Test type	Smartphone location	Movement	Recording length	Number of samples
1	Bicycle	Riding	45-70 s	36
2	Bicycle	Walking	90-110 s	4
3	Bicycle	Standing	300 s	1
4	Footbridge	No movement	300 s	1

It is highlighted that this proof-of-concept study is conducted under the following assumptions:

- All the recording samples are collected throughout the bridge without interrupting, stopping, and/or going back. Although the KF allows realigning the data to the physical location where it was collected (see Section 3.1), more complex actions, such as stopping and returning, may increase the noise level in the recorded dataset. However, in a long-term crowdsourced application, the effects of these types of anomalies would be mitigated. Also, some rules (in terms of time to cross the bridge and/or speed variability) could be included to discard particular recordings.
- The bridge is lively and constantly excited by pedestrians, traffic underneath, and/or wind. As in the previous case, some rules could select only the samples where the recorded vibration in the RoI exceeds a given threshold.
- One single vehicle and one single user are involved in the experimental campaign. Although different bicycles and body properties can potentially vary the identified parameters, in the case of shared vehicles, they are likely to have almost uniform properties.
- No vehicle-bridge interaction or roughness effects have been considered (see Section 4.3.1 for further details).

Moreover, it is assumed that the shift in resonant frequencies due to environmental variation and early damage are always included within the selected RoI. For urban bridges, a polymeric or wooden pavement is much less sensitive to temperature variations compared to asphalt, which is one of the the most well-known sources of variation in modal parameters for regular bridges [67]. Nevertheless, in general, environmental variations affect natural frequencies less than 10% for these types of structures [68]. Thereby, a sufficiently wide RoI (i.e., the natural frequency estimated in a previous identification process ± 10 -20%) should be sufficient to avoid issues related to the frequency shifts that the structure could undergo during the monitoring process.

4.3 Results

The time series of the vertical accelerations recorded during all the tests are used to retrieve the main modal parameters of the structure. The identification of the modal amplitudes is carried out using multiple sensor data (i.e., acceleration, angular velocity, magnetic field, and position) recorded according to the test type 1 and processed using the procedure described in Section 3.

4.3.1 Natural frequencies

Figure 6(a) displays the power spectra of the 42 vertical acceleration time series collected during all the tests described in Table 2. Test type 4 is not affected by human action (riding or walking), bicycle dynamics (vehicle-bridge interaction), or road roughness and is used as a reference recording. As shown in the figure, riding and walking test types have a higher level of noise with respect to the other tests due to the moving vehicle and the user action. However, an accurate estimate of the resonant frequency can be calculated for all the test types by extracting the maxima of the frequency spectra of vertical acceleration in an RoI between 2.2 Hz and 2.8 Hz (selected as 2.5 ± 0.3 Hz, based on the reference frequencies identified in a previous study [63] and reported in Figure 4). The frequencies identified in this study are reported in Figure 6(b) as orange circles. All the frequencies identified using measurements of both the moving and the static sensors are in agreement with the reference values. This shows that the human biomechanics and the pavement roughness do not significantly affect the identification results in this application. In fact, the pavement of pedestrian bridges is typically smooth, and the speed of bicycles is generally low, thus reducing the effects of the road surface profile on the recorded response [10,30]. As mentioned in Section 3, the dynamic parameters identified by the procedure proposed in this paper are average values over a given frequency range. Thereby closely spaced modes, in general, cannot be distinguished. Figure 6(c) shows the statistical distribution of the resonant frequencies identified using test types 1 and 2. The mean of this distribution is 2.533 Hz, and its standard deviation is 0.035 Hz.

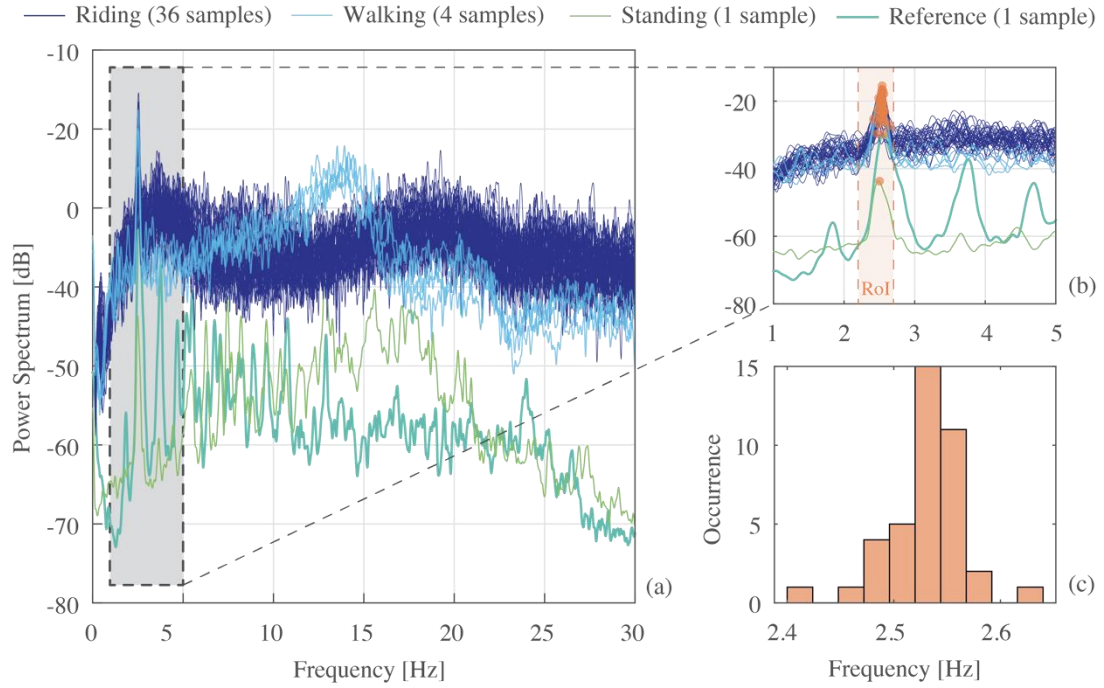


Figure 6 Power spectra relevant to different test types (a), identified frequency values (orange circles) in a zoom view (b), and statistical distribution of the identified results (c)

4.3.2 Modal amplitudes

The vertical acceleration data of test type 1 is also employed, as explained in Section 3, to identify modal amplitudes. As mentioned in the previous section, closely spaced modes cannot be distinguished by the proposed procedure and the shape identified in each frequency range is a combination of the ODSs in that range. Further to this, as mentioned in Section 3, the proposed procedure allows identifying the absolute values of the operational shapes amplitudes but not their signs; thereby, a symmetric and anti-symmetric mode, such as those in Figure 4, cannot be distinguished. However, it must be noted that the final goal of the procedure proposed herein is to use the information extracted from the measurements to identify the onset of possible damage. Local damage affects all the operational and mode shapes at the damage location, except those with a node at that location. This means that the shape identified using the procedure proposed herein, which is a combination of ODSs, is affected by damage and can be used for its identification. In the case of the considered bridge, the similarity of the two mode shapes (Figure 4) makes the procedure more robust since their absolute values are very close, almost coincident. Thereby, the effect of possible damage will be reflected in both of them.

In this study, the amplitude information corresponding to the first two modes of the bridge is extracted by filtering the acceleration time history through a narrow band-pass filter with lower and upper cutoff frequencies equal to 2.2 Hz and 2.8 Hz, respectively. The amplitude is then extracted through the Hilbert transform and converted from time to space domain. To this aim, the DC-EKF illustrated in Section 3.1 is employed to estimate, with a high spatial resolution, the path of the moving bicycle. The path is sampled at 100 Hz, as the vertical acceleration measurements. In the initialization

step, the initial quaternion orientation, position, and magnetic field values of the state vector are set to the values obtained from a reference direction, while other quantities are set to 0. The reference direction was calculated a priori, simply connecting the two ends of the bridge. This way, assuming that the bicycle is aligned with the bridge axis when it enters and leaves the structure, the EKF converges rapidly due to fewer uncertainties on the initial parameters. Moreover, since the magnetic field recording was very noisy, the initial values of additive noise have been set relatively high. However, in practical applications, the data collection would start a while before entering the bridge. Therefore, there would be enough time for the initial parameters and corresponding noise values to be well-calibrated. Table 3 shows the additive noise values used in this application for each state element. The initial state covariance was assumed as a diagonal matrix with nonzero elements equal to 10^{-3} .

The initial and final instants of the measurements used in this procedure were selected by observing the vertical acceleration time history. Figure 7 shows that prominent peaks occur when passing over the expansion joints at the ends of the bridge. However, the entry peak also affects the collected data since a transient vibration component due to the bicycle dynamics is generated. This component generally vanishes within about 3 s in this case study.

Table 3 Initial additive noise variance of the state elements

State element	Noise variance
Quaternion	$1 \cdot 10^{-1}$
Acceleration	$5 \cdot 10^{-3} \text{ m}^2/\text{s}^4$
Angular velocity	$3 \cdot 10^{-6} \text{ rad}^2/\text{s}^2$
Magnetic field	$1 \cdot 10^{-1} \mu\text{T}^2$
Position	$1 \cdot 10^{-6} \text{ m}^2$
Accelerometer bias	$3 \cdot 10^{-1} \text{ m}^2/\text{s}^4$
Gyroscope bias	$3 \cdot 10^{-3} \text{ rad}^2/\text{s}^2$
Magnetometer bias	$20 \mu\text{T}^2$

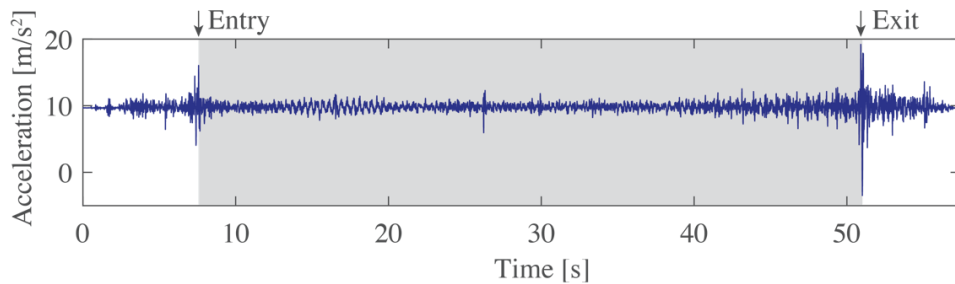


Figure 7 Selection of the interval of interest based on vertical acceleration peaks

Figure 8 shows the densely reconstructed positions (namely, “sample paths”) obtained through the EKF. In this figure, the reference line represents the longitudinal axis of the bridge, and the time-varying instantaneous vehicle speed is represented using the colormap reported on the right-hand side. It is possible to observe a spatial scattering due to inaccuracies of the reconstruction, especially in the central part, where the footbridge becomes narrower. Moreover, due to the less frequent sampling of GPS location, some paths have small jumps in their shape. It should be noted that these jumps are mainly in the direction orthogonal to the reference line. Therefore, they slightly affect the principal paths along the longitudinal bridge axis obtained through PCA.

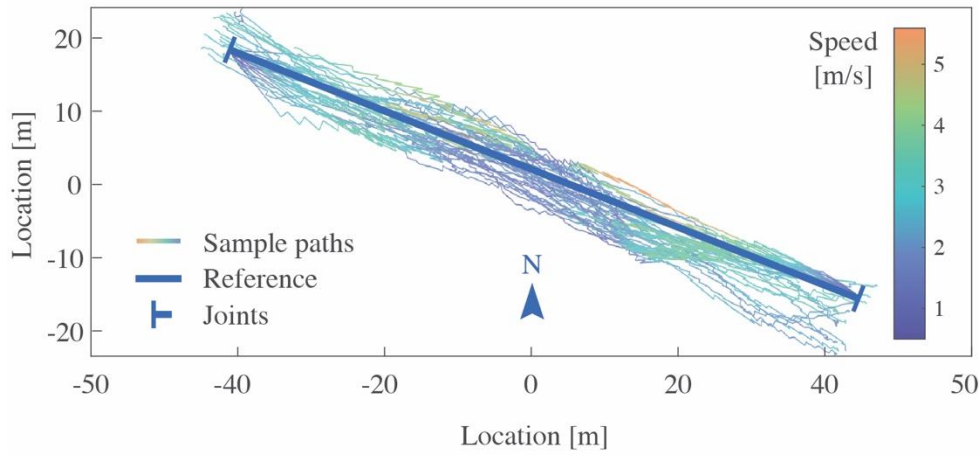


Figure 8 Reference and estimated crossing path

The main steps of the procedure proposed in this paper for reconstructing the ODS associated with the selected frequency RoI are shown in Figure 9. First, the vertical acceleration data (Figure 9(a)) is filtered (Figure 9(b)), and its amplitude is calculated as the absolute value of the related analytic signal (Figure 9(c)). Then, interpolating the modal amplitudes of each sample along with the related principal paths projected on the bridge axis leads to a time-to-space conversion (Figure 9(d)), as explained in Section 3.3. All the irregularities of the reconstructed profile are due to recording noise, as well as to the disturbance generated by the operational conditions (i.e., runners’ excitation), cyclist movements, and road surface variability. However, as demonstrated by Champoux et al. [69], the resonant frequencies of an average bicycle are mostly over 20 Hz and thus very different from those of typical bridges. Therefore, the vehicle characteristics are effectively removed from the recorded response by means of the filtering procedure [70].

Walking typically generates a narrow-band excitation that varies with walking/running speed [39]. If pedestrian force excites the structure in the frequency RoI, the structure is likely to resonate, thus producing a high vibration response that is beneficial to structural identification. In crowdsourcing applications, pedestrians are likely to walk at variable speeds, and walking excitation is generally mixed with other sources, such as traffic and wind. The availability of large sets of modal parameters,

identified from crowdsourced responses, enables averaging out the effect of the variability in the source of vibration and obtaining an accurate estimate of the modal parameters.

The sample shape reported in Figure 9(c)-(d) shows the dynamic effect on the collected acceleration measurement due to the first expansion joint. It is possible to observe that in the left part of the figure, between 0 and 2.5 s (Figure 9(c)), a steeply decreasing acceleration amplitude is recorded due to the free vibration response of the bicycle system following the impulsive excitation generated while overcoming the joint.

All the sample shape amplitudes are finally superimposed, as shown in Figure 10, and the average can be calculated at a user-selected spatial grid through interpolation. In this study, 100 equally spaced amplitude values projected on the bridge longitudinal axis were computed, as reported in Figure 10 in dark blue. This result represents the average ODS computed in the frequency RoI obtained from the 36 samples of test 1. Therefore, it represents the absolute values of the modal shape amplitudes of the first two closely spaced modes. The identified profile is in good accordance with the reference first mode shape, especially for the central part, as represented in Figure 10. It is indeed possible to notice a slight asymmetry in the shape that presents higher amplitudes on the left-hand side. The terminal portions of the identified profile (i.e., below -45 m and over +45 m) are not reported in the figure since they are affected by the free vibration of the bicycle generated by the passage on the expansion joints. As noted by Siringoringo and Fujino, vehicle bounce and pitch motions could hide the bridge response [27]; thereby, it is generally recommended to discard the signal collected close to expansion joints. It should be noted that since bicycles are generally slower than regular vehicles, these intervals are relatively short and do not significantly reduce the inspection range. On the other hand, the considerable reduction of the inspection range due to vehicle dynamics is a well-known issue for cars and trucks [33]. Also, due to slight inaccuracies in the acquisition process, some sample shapes are slightly shorter than others. The average shape has been computed only at the points all the 36 sample shapes are available.

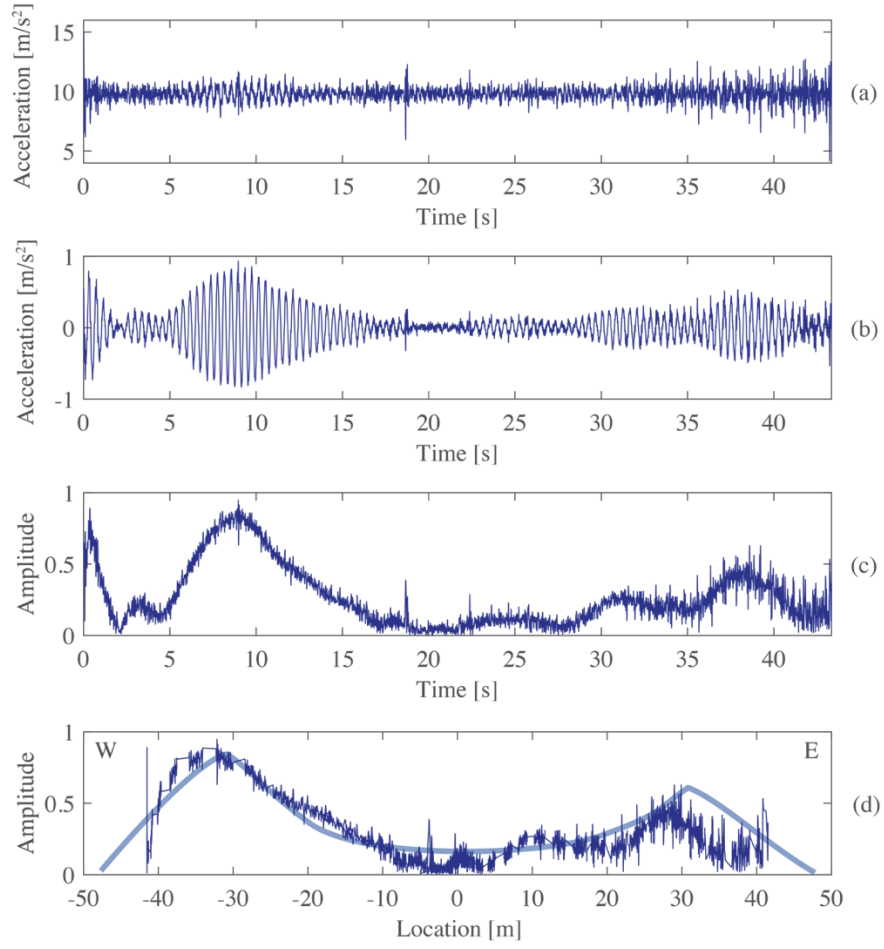


Figure 9 Steps of the procedure for a data sample: (a) vertical acceleration, (b) filtered signal, (c) filtered amplitude, (d) reconstructed sample shape

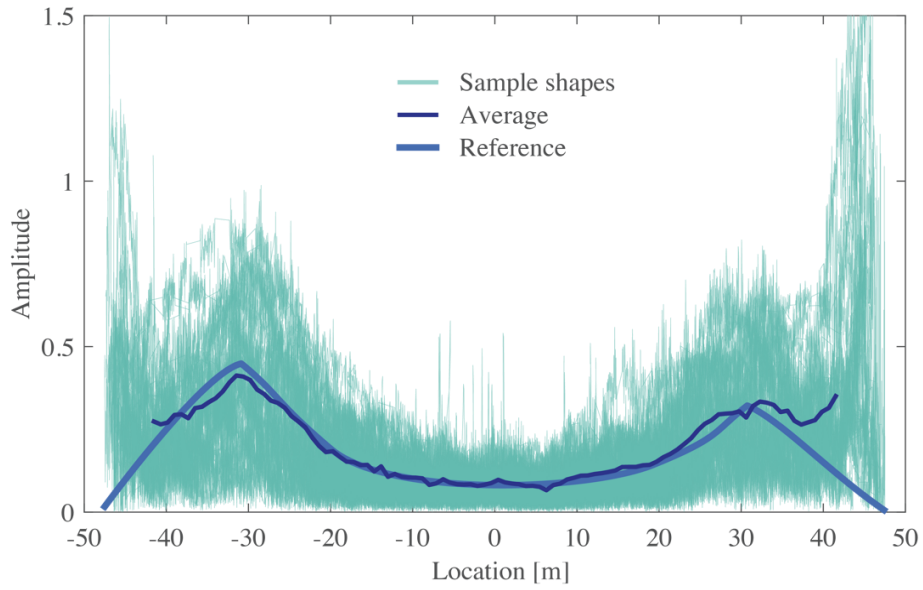


Figure 10 Reference and identified modal amplitude

Due to the relatively low performances of smartphone sensors and on the variable nature of operation conditions and vehicle effects on the collected measures, individual samples do not provide reliable results if used for structural identification. Moreover, due to technical issues, data collection could be discontinuous, especially for older smartphone models. However, in a crowdsensing application, the high number of identified features reduces the uncertainty of the identified values. In this study, a preliminary feasibility analysis has been conducted considering only 36 samples; however, through hundreds of datasets collected by different users in a crowdsourcing strategy, the identified features are likely to improve further. Moreover, a simple procedure can be designed to facilitate the automatic acquisition of the samples based on the identification of the vertical acceleration peaks at the ends of the bridge. This way, the data could be processed in a cloud-based, fully automatic framework. The periodic inspection of the average profile shown in Figure 10 may enable the detection of localized changes, possibly related to structural damage, that can motivate the owners of the infrastructure to arrange further inspections. The reader can refer to exhaustive literature [1,2,59,61] for the employment of the identified damage-sensitive features for damage identification, which goes beyond the scope of this paper.

5. Conclusions

This paper presents a pilot study to demonstrate the practicability of using drive-in smartphone data collected by citizens who drive micromobility light vehicles (e.g., bicycles and kick scooters) to extract dynamic features of urban bridges, such as natural frequencies and modal amplitudes. Human-powered vehicles have never been considered for the health assessment of civil structures, and this work constitutes a first step toward the adoption of light vehicles in indirect structural health monitoring applications. The main advantages of shared bicycles over other types of vehicles include the following aspects:

- Relatively low speed of the micromobility vehicles allows the acquisition of longer datasets, minimizing vehicle vibration close to the expansion joints and reducing the effects of pavement roughness on the collected response.
- High resonant frequencies of the bicycles (due to their low mass and high stiffness) are generally distant from the first fundamental frequencies of the inspected bridges, making the filtering procedure particularly effective for removing the vehicle dynamic effects from the collected response.
- Shared bicycles, differently from private cars, are generally all identical. The effect of their dynamic characteristics on the response recorded by the smartphone can be studied and removed from the signal if needed.
- Bicycles can access almost all the urban bridges, even those that are not accessible by cars.

This study proposes a novel automatic strategy based on the GPS and IMU measurements collected by regular smartphones. An extended Kalman filter and a simple band-pass filtering procedure are the only tools employed in the proposed strategy, making it particularly suitable for cloud processing.

The results obtained for a real footbridge situated in Bologna (Italy) show that, although single datasets collected by each vehicle can be particularly noisy, a crowdsensing-based strategy may provide features that can be potentially employed for monitoring urban infrastructures at a territorial scale. Data collected during different activities, such as standing, walking, and riding on the bridge, have shown the possibility of clearly identify the first natural frequency of the bridge. Moreover, using the retrieved frequency value to design a suitable band-pass filter enables the identification of the absolute value of the modal amplitudes, enclosing information of the first two closely spaced modes. The results are in good accordance with the profile identified in previous studies.

This paper is a proof of concept that shows the possibility of identifying dense mode shapes using shared light vehicles. Dense estimates of mode shapes could be particularly useful to localize structural damage. Specifically, since the presented method provides the modal or operational shapes, all the damage detection techniques based on these parameters or their derivatives can be applied. Further studies must be conducted considering other vehicles and environments and addressing the limitations that characterize monitoring approaches based on modal parameters. Nevertheless, the proposed strategy can be particularly convenient for monitoring infrastructures in large areas since it does not require any deployments of traditional sensing systems and motivates citizens to take care of the urban environment, opening incredible possibilities for planning gamification and reward-based strategies in the monitoring process.

Appendix A: Structure of the extended Kalman filter

The state vector \mathbf{x} and the state transition function $g(\mathbf{x})$ of the DC-EKF described in Section 3.1 have the following structure that depends on the geometrical and the physical relations between the measured variables [71]:

$$\mathbf{x} = \begin{bmatrix} \rho_0 \\ \rho_1 \\ \rho_2 \\ \rho_3 \\ \alpha_1 \\ \alpha_2 \\ \alpha_3 \\ \theta_1 \\ \theta_2 \\ \theta_3 \\ \sigma_1 \\ \sigma_2 \\ \sigma_3 \\ \eta_1 \\ \eta_2 \\ \eta_3 \\ v_1 \\ v_2 \\ v_3 \\ \bar{\alpha}_1 \\ \bar{\alpha}_2 \\ \bar{\alpha}_3 \\ \bar{\theta}_1 \\ \bar{\theta}_2 \\ \bar{\theta}_3 \\ \bar{\sigma}_1 \\ \bar{\sigma}_2 \\ \bar{\sigma}_3 \end{bmatrix}, \quad g(\mathbf{x}) = \begin{bmatrix} -\frac{\rho_1\theta_1 + \rho_2\theta_2 + \rho_3\theta_3}{2} \\ -\frac{\rho_0\theta_1 + \rho_3\theta_2 + \rho_1\theta_3}{2} \\ -\frac{\rho_3\theta_1 + \rho_0\theta_2 + \rho_1\theta_3}{2} \\ -\frac{\rho_1\theta_1 + \rho_2\theta_2 + \rho_0\theta_3}{2} \\ 2 \\ 0 \\ 0 \\ 0 \\ 0 \\ 0 \\ 0 \\ 0 \\ 0 \\ 0 \\ 0 \\ 0 \\ 0 \\ v_1 \\ v_2 \\ v_3 \\ \alpha_1 \\ \alpha_2 \\ \alpha_3 \\ 0 \\ 0 \\ 0 \\ 0 \\ 0 \\ 0 \\ 0 \\ 0 \end{bmatrix} \quad (\text{A.1})$$

The meaning of the symbols used in these expressions is reported in Table 4, and the directions of measurement are illustrated in Figure 11.

Table 4 Measurement symbols

Measurement	Symbol
Quaternion	$\rho_0, \rho_1, \rho_2, \rho_3$
Acceleration (IMU)	$\alpha_1, \alpha_2, \alpha_3$
Angular velocity (IMU)	$\theta_1, \theta_2, \theta_3$
Magnetic field (IMU)	$\sigma_1, \sigma_2, \sigma_3$
Position (GPS)	η_1, η_2, η_3
Velocity (GPS)	v_1, v_2, v_3
Accelerometer bias	$\bar{\alpha}_1, \bar{\alpha}_2, \bar{\alpha}_3$
Gyroscope bias	$\bar{\theta}_1, \bar{\theta}_2, \bar{\theta}_3$
Magnetometer bias	$\bar{\sigma}_1, \bar{\sigma}_2, \bar{\sigma}_3$

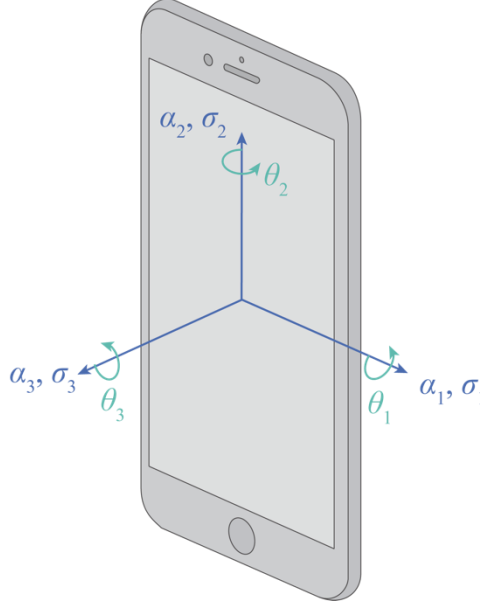


Figure 11 Directions of measurement

The function $g(\mathbf{x})$ describes the evolution of the state vector in time and computes, therefore, its derivative. It is noted that, in the model used in this study, the IMU measurements are expected to be constant while the vehicle moves. Therefore, the elements from the 5-th to the 13-th of the state transition function are taken as zero. Similarly, the model assumes all the biases constant over time, with a null derivative. On the other hand, the derivative of the GPS position is modeled as the measured GPS velocity, the derivative of which, in turn, is the acceleration measured by the MEMS accelerometer.

The observation function has a structure that depends on the quantities included in the measurement vector \mathbf{z}_k . Specifically, if a new acceleration measurement is available ($\mathbf{z}_k = [\alpha_1, \alpha_2, \alpha_3]^T$), the observation function has the following form:

$$h_a(\mathbf{x}) = \begin{bmatrix} \bar{\alpha}_1 - (\alpha_1 - \alpha_{r,1})(q_0^2 + q_1^2 - q_2^2 - q_3^2) - 2(\alpha_2 - \alpha_{r,2})(q_0q_3 + q_1q_2) + 2(\alpha_3 - \alpha_{r,3})(q_0q_2 - q_1q_3) \\ \bar{\alpha}_2 - (\alpha_2 - \alpha_{r,2})(q_0^2 - q_1^2 + q_2^2 - q_3^2) + 2(\alpha_1 - \alpha_{r,1})(q_0q_3 - q_1q_2) - 2(\alpha_3 - \alpha_{r,3})(q_0q_1 + q_2q_3) \\ \bar{\alpha}_3 - (\alpha_3 - \alpha_{r,3})(q_0^2 - q_1^2 - q_2^2 + q_3^2) - 2(\alpha_1 - \alpha_{r,1})(q_0q_2 + q_1q_3) + 2(\alpha_2 - \alpha_{r,2})(q_0q_1 - q_2q_3) \end{bmatrix} \quad (\text{A.2})$$

with $\alpha_{r,1}$ being a reference acceleration measured by the mobile application at the beginning of the measurement process. Conversely, for angular velocity measurements ($\mathbf{z}_k = [\theta_1, \theta_2, \theta_3]^T$), the observation function becomes:

$$h_\theta(\mathbf{x}) = \begin{bmatrix} \bar{\theta}_1 + \theta_1 \\ \bar{\theta}_2 + \theta_2 \\ \bar{\theta}_3 + \theta_3 \end{bmatrix} \quad (\text{A.3})$$

While for magnetic field measurements ($\mathbf{z}_k = [\sigma_1, \sigma_2, \sigma_3]^T$):

$$h_\sigma(\mathbf{x}) = \begin{bmatrix} \bar{\sigma}_1 + \sigma_1(q_0^2 + q_1^2 - q_2^2 - q_3^2) + 2\sigma_2(q_0q_3 + q_1q_2) - 2\sigma_3(q_0q_2 - q_1q_3) \\ \bar{\sigma}_2 + \sigma_2(q_0^2 - q_1^2 + q_2^2 - q_3^2) - 2\sigma_1(q_0q_3 - q_1q_2) + 2\sigma_3(q_0q_1 + q_2q_3) \\ \bar{\sigma}_3 + \sigma_3(q_0^2 - q_1^2 - q_2^2 + q_3^2) + 2\sigma_1(q_0q_2 + q_1q_3) - 2\sigma_2(q_0q_1 - q_2q_3) \end{bmatrix} \quad (\text{A.4})$$

It should be noted that in the cases of acceleration and magnetic field, the measured components are projected onto the vehicle orientation. Besides, a bias is added to all the measurements. Concerning the GPS position data ($\mathbf{z}_k = [\eta_1, \eta_2, \eta_3]^T$), the observation function simply takes the measurement information:

$$h_\eta(\mathbf{x}) = \begin{bmatrix} \eta_1 \\ \eta_2 \\ \eta_3 \end{bmatrix} \quad (\text{A.5})$$

Appendix B: Implementation of the extended Kalman filter

Let $\hat{\mathbf{x}}_{n|m}$ and $\mathbf{P}_{n|m}$ represent the estimate of \mathbf{x} and of the state covariance matrix \mathbf{P} at time t_n , respectively, given the observations up to the instant t_m . In general, the selection of $\hat{\mathbf{x}}_{0|0}$ and $\mathbf{P}_{0|0}$, that denote the initialization state and covariance, can be performed randomly or considering a priori information about the characteristics of the system at the instant t_0 . In this study, the state vector elements are set as the measurements collected by the smartphone when the vehicle passes on the first expansion joint, i.e., when it enters the bridge.

The prediction step consists of solving

$$\begin{cases} \dot{\hat{\mathbf{x}}}(t) = g(\hat{\mathbf{x}}(t)) \\ \dot{\mathbf{P}}(t) = \mathbf{G}(t)\mathbf{P}(t) + \mathbf{P}(t)\mathbf{G}(t)^T + \mathbf{Q}(t) \end{cases} \quad (\text{B.1})$$

where $\dot{\hat{\mathbf{x}}}(t)$ and $\dot{\mathbf{P}}(t)$ indicate the time derivatives of the estimated state vector and state covariance matrix, respectively, and the state transition function is linearized as the Jacobian

$$\mathbf{G}(t) = \left. \frac{\partial g}{\partial \mathbf{x}} \right|_{\hat{\mathbf{x}}(t)} \quad (\text{B.2})$$

Eq. (B.1) is solved considering the initial conditions $\hat{\mathbf{x}}(t_{k-1}) = \mathbf{x}_{k-1|k-1}$ and $\mathbf{P}(t_{k-1}) = \mathbf{P}_{k-1|k-1}$ evaluated at the time instant of the last measurement t_{k-1} , until the next measurement (at time t_k) is available. At this instant, the a priori estimate (i.e., not including yet measurement information at time t) of the current state $\hat{\mathbf{x}}_{k|k-1}$ and covariance $\mathbf{P}_{k|k-1}$ are defined as

$$\begin{cases} \hat{\mathbf{x}}_{k|k-1} = \mathbf{x}(t_k) \\ \mathbf{P}_{k|k-1} = \mathbf{P}(t_k) \end{cases} \quad (\text{B.3})$$

As mentioned in Section 3.1, a constant frequency f_s , equal to the sampling frequency of the vertical acceleration, is selected to calculate the prediction step.

In the update step, the a priori prediction of the current state is combined with the measurement collected at time t_k to refine its estimate. This step consists of evaluating the near-optimal Kalman gain \mathbf{K}_k , which is employed in calculating the updated (a posteriori) state $\hat{\mathbf{x}}_{k|k}$ and covariance $\mathbf{P}_{k|k}$ estimates, as follows:

$$\mathbf{K}_k = \mathbf{P}_{k|k-1} \mathbf{H}_k^T (\mathbf{H}_k \mathbf{P}_{k|k-1} \mathbf{H}_k^T + \mathbf{R}_k)^{-1} \quad (\text{B.4})$$

$$\hat{\mathbf{x}}_{k|k} = \hat{\mathbf{x}}_{k|k-1} + \mathbf{K}_k \left(\mathbf{z}_k - h(\hat{\mathbf{x}}_{k|k-1}) \right) \quad (\text{B.5})$$

$$\mathbf{P}_{k|k} = (\mathbf{I} - \mathbf{K}_k \mathbf{H}_k) \mathbf{P}_{k|k-1} \quad (\text{B.6})$$

where \mathbf{I} indicates an identity matrix. In this case, the observation matrix \mathbf{H}_k is defined as the Jacobian

$$\mathbf{H}_k = \left. \frac{\partial h}{\partial \mathbf{x}} \right|_{\hat{\mathbf{x}}_{k|k-1}} \quad (\text{B.7})$$

Funding

This research did not receive any specific grant from funding agencies in the public, commercial, or not-for-profit sectors.

Compliance with Ethical Standards

The authors declare that they have no conflict of interest.

References

- [1] C.R. Farrar, K. Worden, An introduction to structural health monitoring, *Philosophical Transactions of the Royal Society A: Mathematical, Physical and Engineering Sciences*. 365 (2007) pp. 303–315. <https://doi.org/10.1098/rsta.2006.1928>.
- [2] W. Fan, P. Qiao, Vibration-based damage identification methods: A review and comparative study, *Structural Health Monitoring*. 10 (2011) pp. 83–111. <https://doi.org/10.1177/1475921710365419>.
- [3] S. Quqa, P.F. Giordano, M.P. Limongelli, L. Landi, P.P. Diotallevi, Clump interpolation error for the identification of damage using decentralized sensor networks, *Smart Structures and Systems*. 27 (2021) pp. 351–363. <https://doi.org/10.12989/sss.2021.27.2.351>.
- [4] P.F. Giordano, F. Ubertini, N. Cavalagli, A. Kita, M.G. Masciotta, Four years of structural health monitoring of the San Pietro bell tower in Perugia, Italy: Two years before the earthquake versus two years after, *International Journal of Masonry Research and Innovation*. 5 (2020) pp. 445–467. <https://doi.org/10.1504/IJMRI.2020.111797>.
- [5] F. Magalhães, A. Cunha, E. Caetano, Vibration based structural health monitoring of an arch bridge: From automated OMA to damage detection, *Mechanical Systems and Signal Processing*. 28 (2012) pp. 212–228. <https://doi.org/10.1016/j.ymssp.2011.06.011>.
- [6] M.P. Limongelli, E. Chatzi, M. Döhler, G. Lombaert, E. Reynders, Towards extraction of

- vibration-based damage indicators, in: EWSHM-8th European Workshop on Structural Health Monitoring, pp. 546-555, 2016. ISBN: 978-151082793-6.
- [7] P.F. Giordano, M.P. Limongelli, The value of structural health monitoring in seismic emergency management of bridges, *Structure and Infrastructure Engineering*. (2020) pp. 1–17. <https://doi.org/10.1080/15732479.2020.1862251>.
 - [8] D. Zonta, B. Glisic, S. Adriaenssens, Value of information: impact of monitoring on decision-making, *Structural Control and Health Monitoring*. 21 (2014) pp. 1043–1056. <https://doi.org/10.1002/stc.1631>.
 - [9] Y.B. Yang, C.W. Lin, J.D. Yau, Extracting bridge frequencies from the dynamic response of a passing vehicle, *Journal of Sound and Vibration*. 272 (2004) 471–493. [https://doi.org/10.1016/S0022-460X\(03\)00378-X](https://doi.org/10.1016/S0022-460X(03)00378-X).
 - [10] C.W. Lin, Y.B. Yang, Use of a passing vehicle to scan the fundamental bridge frequencies: An experimental verification, *Engineering Structures*. 27 (2005) pp. 1865–1878. <https://doi.org/10.1016/j.engstruct.2005.06.016>.
 - [11] C.W. Kim, M. Kawatani, Challenge for a drive-by bridge inspection, in: H. Furuta, D. Frangopol, M. Shinozuka (Eds.), *Safety, Reliability and Risk of Structures, Infrastructures and Engineering Systems*, Taylor & Francis, Osaka, Japan, 2009: pp. 758–765. <https://doi.org/10.1201/9780367803667>.
 - [12] F. Cerda, J. Garrett, J. Bielak, J. Barrera, Z. Zhuang, S. Chen, M. McCann, J. Kovačević, P. Rizzo, Indirect structural health monitoring in bridges: Scale experiments, *Bridge Maintenance, Safety, Management, Resilience and Sustainability - Proceedings of the Sixth International Conference on Bridge Maintenance, Safety and Management*, 2012: pp. 346–353. ISBN: 978-041562124-3.
 - [13] C.W. Kim, S. Inoue, K. Sugiura, P.J. McGetrick, M. Kawatani, Extracting bridge frequencies from dynamic responses of two passing vehicles, in: *Insights and Innovations in Structural Engineering, Mechanics and Computation - Proceedings of the 6th International Conference on Structural Engineering, Mechanics and Computation, SEMC 2016*, 2016: pp. 1858-1864. <https://doi.org/10.1201/9781315641645-307>.
 - [14] J. Li, X. Zhu, S. seong Law, B. Samali, Indirect bridge modal parameters identification with one stationary and one moving sensors and stochastic subspace identification, *Journal of Sound and Vibration*. 446 (2019) pp. 1-21. <https://doi.org/10.1016/j.jsv.2019.01.024>.
 - [15] J. Kim, J.P. Lynch, Experimental analysis of vehiclebridge interaction using a wireless monitoring system and a two-stage system identification technique, *Mechanical Systems and Signal Processing*. 28 (2012) pp. 3-19. <https://doi.org/10.1016/j.ymssp.2011.12.008>.

- [16] S. Sadeghi Eshkevari, T.J. Matarazzo, S.N. Pakzad, Bridge modal identification using acceleration measurements within moving vehicles, *Mechanical Systems and Signal Processing*. 141 (2020) 106733. <https://doi.org/10.1016/j.ymssp.2020.106733>.
- [17] A. González, E.J. Obrien, P.J. McGetrick, Identification of damping in a bridge using a moving instrumented vehicle, *Journal of Sound and Vibration*. 331 (2012) pp. 4115–4131. <https://doi.org/10.1016/j.jsv.2012.04.019>.
- [18] S. Ercolessi, G. Fabbrocino, C. Rainieri, Indirect Measurements of Bridge Vibrations as an Experimental Tool Supporting Periodic Inspections, *Infrastructures*. 6 (2021) 39. <https://doi.org/10.3390/infrastructures6030039>.
- [19] Y. Oshima, K. Yamamoto, K. Sugiura, Damage assessment of a bridge based on mode shapes estimated by responses of passing vehicles, *Smart Structures and Systems*. 13 (2014) pp. 731–753. <https://doi.org/10.12989/sss.2014.13.5.731>.
- [20] J. Liu, S. Chen, M. Bergés, J. Bielak, J.H. Garrett, J. Kovačević, H.Y. Noh, Diagnosis algorithms for indirect structural health monitoring of a bridge model via dimensionality reduction, *Mechanical Systems and Signal Processing*. 136 (2020) 106454. <https://doi.org/10.1016/j.ymssp.2019.106454>.
- [21] G. Lederman, Z. Wang, J. Bielak, H. Noh, J.H. Garrett, S. Chen, J. Kovačević, F. Cerda, P. Rizzo, Damage quantification and localization algorithms for indirect SHM of bridges, in: *Bridge Maintenance, Safety, Management and Life Extension - Proceedings of the 7th International Conference of Bridge Maintenance, Safety and Management*, pp. 640-647, IABMAS 2014, 2014. <https://doi.org/10.1201/b17063-93>.
- [22] C.W. Kim, K.C. Chang, P.J. McGetrick, S. Inoue, S. Hasegawa, Utilizing moving vehicles as sensors for bridge condition screening - A laboratory verification, *Sensors and Materials*. 29 (2017) pp. 153-163. <https://doi.org/10.18494/SAM.2017.1433>.
- [23] Y. Bin Yang, W.F. Chen, H.W. Yu, C.S. Chan, Experimental study of a hand-drawn cart for measuring the bridge frequencies, *Engineering Structures*. 57 (2013) pp. 222-231. <https://doi.org/10.1016/j.engstruct.2013.09.007>.
- [24] H. Wang, T. Nagayama, J. Nakasuka, B. Zhao, D. Su, Extraction of bridge fundamental frequency from estimated vehicle excitation through a particle filter approach, *Journal of Sound and Vibration*. 428 (2018) pp. 44-58. <https://doi.org/10.1016/j.jsv.2018.04.030>.
- [25] P.J. McGetrick, C.W. Kim, An indirect bridge inspection method incorporating a wavelet-based damage indicator and pattern recognition, in: *Proceedings of the International Conference on Structural Dynamic*, pp. 2605-2612, EUROLYN, Porto, 2014. ISBN: 978-972752165-4.

- [26] A. Aloisio, R. Alaggio, M. Fragiaco, Bending Stiffness Identification of Simply Supported Girders using an Instrumented Vehicle: Full Scale Tests, Sensitivity Analysis, and Discussion, *Journal of Bridge Engineering*. 26 (2021) 04020115. [https://doi.org/10.1061/\(asce\)be.1943-5592.0001654](https://doi.org/10.1061/(asce)be.1943-5592.0001654).
- [27] D.M. Siringoringo, Y. Fujino, Estimating Bridge Fundamental Frequency from Vibration Response of Instrumented Passing Vehicle: Analytical and Experimental Study, *Advances in Structural Engineering*. 15 (2012) pp. 417–433. <https://doi.org/10.1260/1369-4332.15.3.417>.
- [28] A. Miyamoto, A. Yabe, Development of practical health monitoring system for short- and medium-span bridges based on vibration responses of city bus, *Journal of Civil Structural Health Monitoring*. 2 (2012) pp. 47–63. <https://doi.org/10.1007/s13349-012-0017-0>.
- [29] X.Q. Zhu, S.S. Law, Structural health monitoring based on vehicle-bridge interaction: Accomplishments and challenges, *Advances in Structural Engineering*. 18 (2015) pp. 1999–2015. <https://doi.org/10.1260/1369-4332.18.12.1999>.
- [30] A. Malekjafarian, P.J. McGetrick, E.J. O'Brien, A review of indirect bridge monitoring using passing vehicles, *Shock and Vibration*. 2015 (2015) 286139. <https://doi.org/10.1155/2015/286139>.
- [31] H. Shokravi, H. Shokravi, N. Bakhary, M. Heidarrezaei, S.S. Rahimian Koloor, M. Petru, Vehicle-Assisted Techniques for Health Monitoring of Bridges, *Sensors*. 20 (2020) 3460. <https://doi.org/10.3390/s20123460>.
- [32] M. Feng, Y. Fukuda, M. Mizuta, E. Ozer, Citizen sensors for SHM: Use of accelerometer data from smartphones, *Sensors*. 15 (2015) pp.2980-2998. <https://doi.org/10.3390/s150202980>.
- [33] P.J. McGetrick, D. Hester, S.E. Taylor, Implementation of a drive-by monitoring system for transport infrastructure utilising smartphone technology and GNSS, *Journal of Civil Structural Health Monitoring*. 7 (2017) pp. 175-189. <https://doi.org/10.1007/s13349-017-0218-7>.
- [34] A. Elhatab, N. Uddin, E. O'Brien, Drive-by bridge damage monitoring using Bridge Displacement Profile Difference, *Journal of Civil Structural Health Monitoring*. 6 (2016) pp. 839–850. <https://doi.org/10.1007/s13349-016-0203-6>.
- [35] E. Ozer, R. Purasinghe, M.Q. Feng, Multi-output modal identification of landmark suspension bridges with distributed smartphone data: Golden Gate Bridge, *Structural Control and Health Monitoring*. 27 (2020) pp. 1–29. <https://doi.org/10.1002/stc.2576>.
- [36] T.J. Matarazzo, P. Santi, S.N. Pakzad, K. Carter, C. Ratti, B. Moaveni, C. Osgood, N. Jacob, Crowdsensing Framework for Monitoring Bridge Vibrations Using Moving Smartphones, *Proceedings of the IEEE*. 106 (2018) pp. 577–593. <https://doi.org/10.1109/JPROC.2018.2808759>.

- [37] Q. Mei, M. Gül, A crowdsourcing-based methodology using smartphones for bridge health monitoring, *Structural Health Monitoring*. 18 (2019) pp. 1602–1619.
<https://doi.org/10.1177/1475921718815457>.
- [38] E. Ozer, M.Q. Feng, D. Feng, Citizen sensors for SHM: Towards a crowdsourcing platform, *Sensors*. 15 (2015) pp. 14591–14614. <https://doi.org/10.3390/s150614591>.
- [39] E. Ozer, M.Q. Feng, Biomechanically influenced mobile and participatory pedestrian data for bridge monitoring, *International Journal of Distributed Sensor Networks*. 13 (2017) 155014771770524. <https://doi.org/10.1177/1550147717705240>.
- [40] E. Ozer, M.Q. Feng, Structural Reliability Estimation with Participatory Sensing and Mobile Cyber-Physical Structural Health Monitoring Systems, *Applied Sciences*. 9 (2019) 2840.
<https://doi.org/10.3390/app9142840>.
- [41] T.J. Matarazzo, D. Kondor, P. Santi, S. Milardo, S.S. Eshkevari, S.N. Pakzad, C. Ratti, Crowdsourcing Bridge Vital Signs with Smartphone Vehicle Trips, *ArXiv* (2020).
<https://arxiv.org/abs/2010.07026>.
- [42] S. Cho, R.K. Giles, B.F. Spencer, System identification of a historic swing truss bridge using a wireless sensor network employing orientation correction, *Structural Control and Health Monitoring*. 22 (2015) pp. 255–272. <https://doi.org/10.1002/stc.1672>.
- [43] H. Sun, O. Büyüköztürk, Identification of traffic-induced nodal excitations of truss bridges through heterogeneous data fusion, *Smart Materials and Structures*. 24 (2015) 075032.
<https://doi.org/10.1088/0964-1726/24/7/075032>.
- [44] E. Ozer, M.Q. Feng, Direction-sensitive smart monitoring of structures using heterogeneous smartphone sensor data and coordinate system transformation, *Smart Materials and Structures*. 26 (2017) 045026. <https://doi.org/10.1088/1361-665X/aa6298>.
- [45] F. Seraj, B.J. Van Der Zwaag, A. Dilo, T. Luarasi, P. Havinga, Roads: A road pavement monitoring system for anomaly detection using smart phones, in: *Lecture Notes in Computer Science (Including Subseries Lecture Notes in Artificial Intelligence and Lecture Notes in Bioinformatics)*, pp.128-146, 2016. https://doi.org/10.1007/978-3-319-29009-6_7.
- [46] T.-Y. Chuang, N.-H. Perng, J.-Y. Han, Pavement performance monitoring and anomaly recognition based on crowdsourcing spatiotemporal data, *Automation in Construction*. 106 (2019) 102882. <https://doi.org/10.1016/j.autcon.2019.102882>.
- [47] S. Mustapha, A. Kassir, K. Hassoun, Z. Dawy, H. Abi-Rached, Estimation of crowd flow and load on pedestrian bridges using machine learning with sensor fusion, *Automation in Construction*. 112 (2020) 103092. <https://doi.org/10.1016/j.autcon.2020.103092>.
- [48] S. Shokouhyar, S. Shokoohyar, A. Sobhani, A.J. Gorizi, Shared mobility in post-COVID era:

- New challenges and opportunities, *Sustainable Cities and Society*. 67 (2021) 102714.
<https://doi.org/10.1016/j.scs.2021.102714>.
- [49] A. Hosseinzadeh, M. Algomaiah, R. Kluger, Z. Li, E-scooters and sustainability: Investigating the relationship between the density of E-scooter trips and characteristics of sustainable urban development, *Sustainable Cities and Society*. 66 (2021) 102624.
<https://doi.org/10.1016/j.scs.2020.102624>.
- [50] T.H. Silva, C.S.F.S. Celes, J.B.B. Neto, V.F.S. Mota, F.D. da Cunha, A.P.G. Ferreira, A.I.J.T. Ribeiro, P.O.S. Vaz de Melo, J.M. Almeida, A.A.F. Loureiro, Users in the urban sensing process, in: *Pervasive Computing*, Elsevier, pp. 45–95, 2016. <https://doi.org/10.1016/B978-0-12-803663-1.00003-6>.
- [51] S. Shaheen, A. Cohen, N. Chan, A. Bansal, Sharing strategies: carsharing, shared micromobility (bikesharing and scooter sharing), transportation network companies, microtransit, and other innovative mobility modes, in: *Transportation, Land Use, and Environmental Planning*, Elsevier, pp. 237–262, 2020. <https://doi.org/10.1016/B978-0-12-815167-9.00013-X>.
- [52] S. Di Dio, M. La Gennusa, G. Peri, G. Rizzo, I. Vinci, Involving people in the building up of smart and sustainable cities: How to influence commuters' behaviors through a mobile app game, *Sustainable Cities and Society*. 42 (2018) pp. 325–336.
<https://doi.org/10.1016/j.scs.2018.07.021>.
- [53] S.J. Julier, J.K. Uhlmann, Unscented filtering and nonlinear estimation, *Proceedings of the IEEE*. 92 (2004) pp. 401–422. <https://doi.org/10.1109/JPROC.2003.823141>.
- [54] G.Y. Kulikov, M. V. Kulikova, Accurate numerical implementation of the continuous-discrete extended kalman filter, *IEEE Transactions on Automatic Control*. 59 (2014) pp. 273–279.
<https://doi.org/10.1109/TAC.2013.2272136>.
- [55] S. Quqa, L. Landi, P.P. Diotallevi, Modal assurance distribution of multivariate signals for modal identification of time-varying dynamic systems, *Mechanical Systems and Signal Processing*. 148 (2021) 107136. <https://doi.org/10.1016/j.ymssp.2020.107136>.
- [56] S. Quqa, L. Landi, P.P. Diotallevi, Automatic identification of dense damage-sensitive features in civil infrastructure using sparse sensor networks, *Automation in Construction*. 128 (2021) 103740. <https://doi.org/10.1016/j.autcon.2021.103740>.
- [57] N.E. Huang, Z. Wu, S.R. Long, K.C. Arnold, X. Chen, K. Blank, On instantaneous frequency, *Advances in Adaptive Data Analysis*. 01 (2009) pp. 177–229.
<https://doi.org/10.1142/S1793536909000096>.
- [58] M.P. Limongelli, Frequency response function interpolation for damage detection under

- changing environment, *Mechanical Systems and Signal Processing*. 24 (2010) pp. 2898-2913.
<https://doi.org/10.1016/j.ymssp.2010.03.004>.
- [59] P.F. Giordano, M.P. Limongelli, Response-based time-invariant methods for damage localization on a concrete bridge, *Structural Concrete*. 21 (2020) pp. 1254–1271.
<https://doi.org/10.1002/suco.202000013>.
- [60] S. Quqa, L. Landi, P.P. Diotallevi, Seismic structural health monitoring using the modal assurance distribution, *Earthquake Engineering & Structural Dynamics*. 50 (2021) pp. 2379-2397. <https://doi.org/10.1002/eqe.3451>.
- [61] M. Dilella, M.P. Limongelli, A. Morassi, Damage localization in bridges via the FRF interpolation method, *Mechanical Systems and Signal Processing*. 52-53 (2015) pp. 162-180.
<https://doi.org/10.1016/j.ymssp.2014.08.014>.
- [62] M. Majowiecki, Three footbridges, in: 2nd International Conference Footbridge 2005, Venice, Italy, December 6-8, 2005.
- [63] M. Majowiecki, N. Cosentino, Experiences on footbridge conceptual design vs. dynamic performances, in: 4th International Conference Footbridge 2011, Wroclaw, Poland, July 6-8, 2011.
- [64] T. Dixon, iPhone SE 2020 Teardown, iFixit. (2020).
<https://www.ifixit.com/Teardown/iPhone+SE+2020+Teardown/133066> (accessed July 9, 2021).
- [65] K. Katevas, Analysing crowd behaviours using mobile sensing, Queen Mary University of London, 2018. <https://qmro.qmul.ac.uk/xmlui/handle/123456789/54059> (accessed October 17, 2021).
- [66] MathWorks, MATLAB Mobile, (2021). <https://uk.mathworks.com/products/matlab-mobile.html> (accessed July 9, 2021).
- [67] H. Nandan, M.P. Singh, Effects of thermal environment on structural frequencies: Part I – A simulation study, *Engineering Structures*. 81 (2014) pp. 480–490.
<https://doi.org/10.1016/j.engstruct.2014.06.046>.
- [68] P. Moser, B. Moaveni, Environmental effects on the identified natural frequencies of the Dowling Hall Footbridge, *Mechanical Systems and Signal Processing*. 25 (2011) pp. 2336–2357. <https://doi.org/10.1016/j.ymssp.2011.03.005>.
- [69] Y. Champoux, S. Richard, J.M. Drouet, Bicycle structural dynamics, *Sound and Vibration*. 41 (2007) pp. 16–24.
- [70] Y.B. Yang, K.C. Chang, Y.C. Li, Filtering techniques for extracting bridge frequencies from a

test vehicle moving over the bridge, *Engineering Structures*. 48 (2013) pp. 353–362.
<https://doi.org/10.1016/j.engstruct.2012.09.025>.

[71] MathWorks, Navigation Toolbox Reference, (2021).

https://www.mathworks.com/help/pdf_doc/nav/nav_ref.pdf (accessed July 9, 2021).